NANOROBOTS

Mobile nanotweezers for active colloidal manipulation

Souvik Ghosh[1] and Ambarish Ghosh[1,2,3]*

An important goal in nanotechnology is to control and manipulate submicrometer objects in fluidic environments, for which optical traps based on strongly localized electromagnetic fields around plasmonic nanostructures can provide a promising solution. Conventional plasmonics based trapping occurs at predefined spots on the surface of a nanopatterned substrate and is severely speed-limited by the diffusion of colloidal objects into the trapping volume. As we demonstrate, these limitations can be overcome by integrating plasmonic nanostructures with magnetically driven helical microrobots and maneuvering the resultant mobile nanotweezers (MNTs) under optical illumination. These nanotweezers can be remotely maneuvered within the bulk fluid and temporarily stamped onto the microfluidic chamber surface. The working range of these MNTs matches that of state-of-the-art plasmonic tweezers and allows selective pickup, transport, release, and positioning of submicrometer objects with great speed and accuracy. The MNTs can be used in standard microfluidic chambers to manipulate one or many nano-objects in three dimensions and are applicable to a variety of materials, including bacteria and fluorescent nanodiamonds. MNTs may allow previously unknown capabilities in optical nanomanipulation by combining the strengths of two recent advances in nanotechnology.

INTRODUCTION

Controlled manipulation of nanoscale objects suspended in fluidic medium is one of the defining goals of modern nanotechnology (*1*). The standard approach is to trap particles using optical (*2*), acoustic (*3*), magnetic (*4*), electric (*5*), or flow fields (*6*), resulting in numerous breakthroughs in biophysics and microfluidics. However, the trapping force decreases with the size of the object, rendering traditional methods inefficient when object sizes are reduced to submicrometer dimensions. Plasmonic tweezers (*7*, *8*), which rely on localized electromagnetic fields near metallic nanostructures, offer an alternative by generating strong trapping forces at low levels of optical illumination and have been used to trap and manipulate particles as small as tens of nanometers (*9*).

Despite plasmonic tweezers offering superior performance (*10*, *11*) in reducing both the size of the trapped object and the required illumination intensity, there are critical disadvantages associated with this otherwise promising technique of optical manipulation. The enhanced electromagnetic field gradient around a plasmonic nanostructure is localized within a small region, typically a fraction of the optical wavelength. Accordingly, trapping relies on the probability of a particle diffusing into a small volume, which is an inefficient process in the absence of other forces (*12*). An additional difficulty arises in maneuvering trapped particles across the microfluidic chamber, which requires large-area nanopatterning of the substrate.

An alternate strategy for manipulation of nanomaterials has been developed in recent years using microrobots (*13*). These are micro- to nanosized motile particles driven by chemical reactions (*14*, *15*) or externally applied magnetic fields (*16*–*18*), which have been used (*19*, *20*) to capture, transport, and release the cargo in lab-on-chip applications. Crucially, the microrobots can be driven quickly and with precise control, overcoming random Brownian fluctuations. Unfortunately, their methods of cargo capture and release rely on chemical functionalization (*21*) and/or having magnetic elements (*22*) in both the microrobot and the cargo, which necessitates a high degree of specificity in their interaction. Alternate efforts, for example, using vortex flow (*6*, *23*–*25*) of magnetic rods, restrict the minimum size of the cargo to 1 μm. Use of optical fields for capturing and releasing the cargo would provide a more general approach applicable to a wide variety of materials. As we demonstrate here, this is possible by combining plasmonic tweezers with microrobots, resulting in mobile nanotweezers (MNTs) whose performance combines the best of both worlds: capturing, maneuvering, and positioning submicrometer objects of various materials at low illumination intensities, high speeds, and with great control.

RESULTS

The microrobots chosen here are based on ferromagnetic, helical nanostructures (*16*) that can be maneuvered by a rotating, homogeneous magnetic field (Fig. 1A). Their motion resembles the way various microorganisms translate by rotating helical flagella (*26*) and offers higher efficiency than maneuvering objects using magnetic field gradients. The spherical head attached to the helical shape is not necessary to achieve controlled motion but is rather related to the chosen method of fabrication (more experimental details are in the Supplementary Materials). A small, rotating magnetic field causes the permanent magnetic moment of the ferromagnetic MNT to rotate synchronously with the field, resulting in a rotation and therefore translation of the nanohelix (like a corkscrew). The direction of motion could be controlled in three dimensions by varying the plane and sense of the rotating field using a triaxial Helmholtz coil. The speed of the helix was proportional to the frequency (Ω_B) of the rotating magnetic field and the hydrodynamic pitch of the helix, provided that the applied magnetic torque was greater than the drag from the surrounding fluid. To impart plasmonic properties, we integrated silver nanostructures with the helices, which resulted in a strongly localized electric field upon optical illumination. We experimented with various MNT designs and report on two main strategies, shown as MNT-D1 and MNT-D2 (Fig. 1B). The key difference between the designs was in the way the plasmonic material was integrated: MNT-D1 contained Ag islands throughout the surface of the helix, whereas the number of Ag elements was significantly lower in MNT-D2. This resulted in stronger thermoplasmonic effects with D1, which greatly influenced the trapping process.

[1]Centre for Nano Science and Engineering, Indian Institute of Science, Bangalore 560012, India. [2]Department of Electrical Communication Engineering, Indian Institute of Science, Bangalore 560012, India. [3]Department of Physics, Indian Institute of Science, Bangalore 560012, India.
*Corresponding author. Email: ambarish@iisc.ac.in

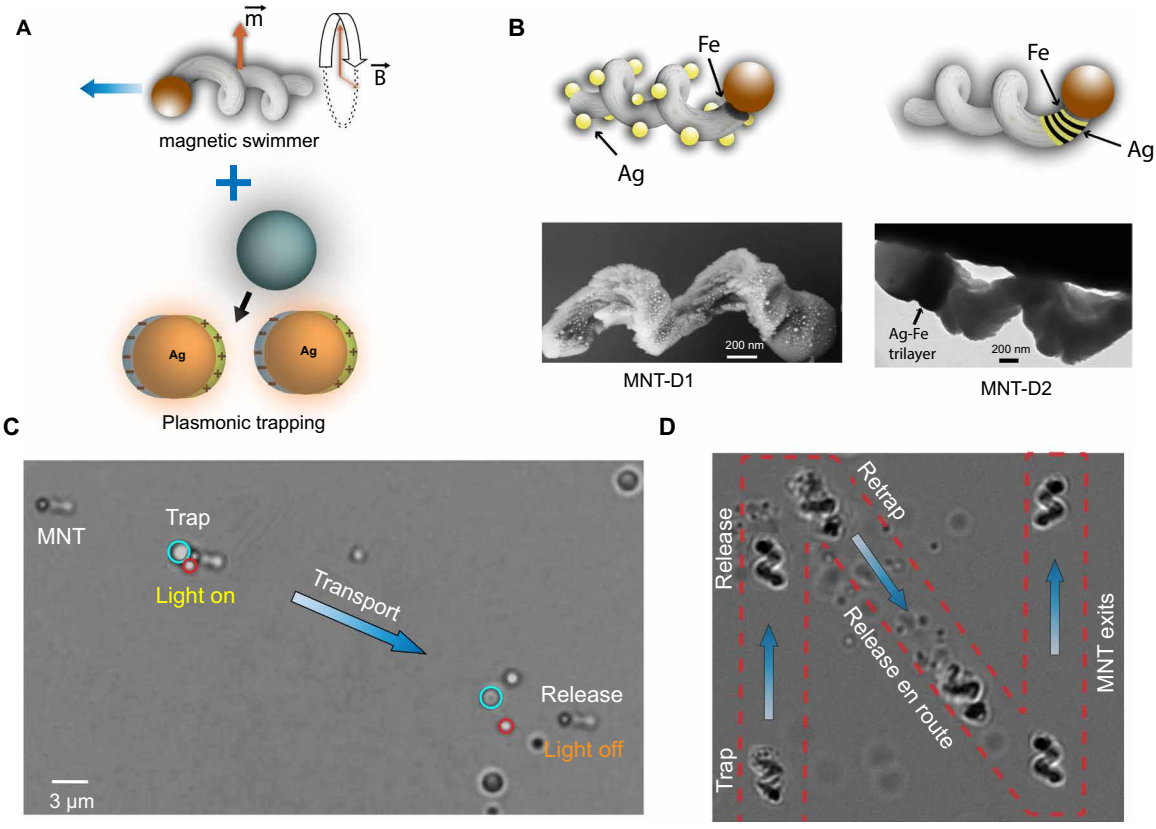

Fig. 1. Mobile nanotweezer. (**A**) Integration of plasmonic nanoparticles with magnetically actuated helical microrobots. The magnetized helical nanostructure can be propelled with small (approximately a few tens of gauss) rotating magnetic fields, whereas the Ag islands upon optical illumination generate strongly localized electric fields that can be used to trap small particles. The shape is crucial to couple magnetically induced rotation of the helix with translation. (**B**) Schematics of MNT-D1 and MNT-D2. Both designs contained iron as the magnetic element integrated with the helical structure. Whereas D1 contained small plasmonic (silver) nanoparticles distributed across its surface, alternating layers of silver (plasmonic) and iron (magnetic) were incorporated within the structure of D2. (**C**) Demonstration of trapping, transporting, and releasing colloidal beads with diameters of 1 and 2 μm over 22 μm (from movie S1). The illumination intensity was 18 kW/cm^2, and the beads were transported at 1.8 μm/s. (**D**) Manipulating a collection of 500-nm silica beads at an intensity of 30 kW/cm^2 to trace out the letter "N." Initially, the entire aggregate of particles was trapped, transported, and released. The collection was trapped again and maneuvered in a different path. The beads were released on the way as the optical intensity was reduced en route. Last, the MNT was driven out of the field of view.

The MNTs were fabricated in large numbers with a yield of greater than 10^8 cm^{-2} of the substrate and could be released by sonicating the substrate in a fluid. The experimental setup has a defocused optical beam and a triaxial Helmholtz coil built around a standard microfluidic device made of glass (fig. S1). The fluidic chamber contains a suspension of MNTs and cargo in the form of colloidal particles. An example of plasmonic trapping of a colloidal bead, and subsequent transport and release, is shown in Fig. 1C and movie S1. The MNTs were driven close to the colloidal particle of interest, and this could be done either in the presence or absence of any illumination. Above a threshold optical power, the beads could get trapped by the MNT, and subsequently, the MNT-bead system could be magnetically steered to the desired location. To release the bead, we reduced the illumination intensity below the threshold value, which depended on the size of the bead and the speed of the MNT-bead system. Our approach circumvents two major disadvantages of optical manipulation with standard plasmonic tweezers: (i) The MNT could be driven toward the particle of interest rather than waiting for it to diffuse into the trap, and (ii) the tasks could be carried out in standard microfluidic chambers that do not require specialized nanopatterned features.

Although we limited these experiments to an area of around 1000 μm^2, in principle, we could maneuver the MNTs, and subsequently trap and release the cargo, anywhere across a microfluidic device of 2 cm × 2 cm. The trapping efficiency of the MNTs matches the efficiency of state-of-the-art plasmonic tweezers, where beads as small as 150 nm under an illumination intensity of 30 kW/cm^2 were maneuvered at 0.7 μm/s (movie S2).

In Fig. 1D, we demonstrate the high spatiotemporal control with which the MNTs could manipulate colloidal particles. A collection of 500-nm silica beads was trapped, transported, and subsequently released in a different spot. The beads were then trapped again, and the MNT was propelled to another location with a reduced optical intensity, thereby releasing the trapped particles en route. Last, the MNT was driven away from the field of view, completing a trajectory along the letter "N" (movie S3). Previous methods of collective transport were limited to either irreversible chemical interaction (*27*) or larger cargo sizes (*23*).

The mechanism of optical trapping for the two MNT designs is shown schematically in Fig. 2A. For both designs, strong, near fields very close (<100) to the MNTs aided the trapping process. The laser wavelength (447 nm) was close to the maximum optical absorption of MNT-D1 (see fig. S3), which caused substantial heating of the MNT. This gave rise to convective flow (*28*) and thermophoretic forces (*29*) on colloids close to MNT-D1, where the thermal gradient (∇T) was high. The direction of thermophoretic force depends on the sign of the Soret coefficient (S_T) of the trapped colloid (*30*) and therefore could either aid or hinder the trapping process. Using numerical simulations, we estimated the temperature rise (Fig. 2B)

and the resultant convective flow (Fig. 2C) for MNT-D1 to be as high as 70°C and 0.2 μm/s, respectively (see fig. S13). The strong convective flow arose from heating many closely placed plasmonic particles on the entire half surface of MNT-D1, as opposed to heating isolated nanostructures in traditional plasmonic tweezer experiments. Under similar experimental conditions, we measured the convective flow velocity to be ~0.3 to 0.4 μm/s around 10 μm away from the MNT, which matches with and therefore validates the overall numerical approach. Although the convective velocity was higher closer to the MNT, the thermal gradient was also high close to the MNT; therefore, the dominant force acting on the colloids was thermophoretic in origin. Additional experiments elucidating the thermophoretic forces close to MNT-D1 are shown in the Supplementary Materials (see fig. S5). In comparison, the amount of plasmonic material was far less in MNT-D2, which showed weaker thermoplasmonic effects.

In Fig. 2D, we compare the relative performance of the two designs and beads of diverse sizes [MNT-D1, silica; MNT-D2, silica and polystyrene (PS)]. The minimum intensity (I_{min}) to trap a bead with a stationary MNT reduced as the bead size was increased. Enhanced heating and corresponding thermophoretic attraction in design D1 allowed silica beads to be trapped at slightly lower laser powers compared with design D2. The magnitudes of I_{min} for silica and PS beads were almost the same for D2, which proved that any heating was negligible. In Fig. 2E, we plot the maximum frequency (Ω_{max}) at which an MNT-bead system can be rotated for a fixed illumination intensity of 22 kW/cm^2. Experiments with MNT-D1 showed that for $\Omega_B \leq \Omega_{max}$, the silica beads were strongly pushed onto the rotating helix, whereas for MNT-D2, the beads (PS and silica) rotated synchronously. This difference was due to the strong thermophoretic force present only with MNT-D1. The measurement of Ω_{max} allowed us to estimate the effective trapping force to be more than 30 fN for both MNT designs at 22 kW/cm^2 (see fig. S14). This is much larger than the Brownian force (*31*) on a suspended colloid, which, for a silica bead of radius r = 150 nm, is given by $F_B = k_B T/r$, which is ~7 fN. Also important is the force from the radiation pressure (*32*) on the colloids, which can be estimated to be around 7 fN for a 1-μm silica bead under 22 kW/cm^2. However, the effect of radiation pressure can be nullified by splitting the incident beam into two equal counter-propagating components (*33*, *34*) and subsequently illuminating the chamber from both top and bottom.

To summarize these observations, MNT-D1 showed strong thermoplasmonic effects, was preferable for materials with positive S_T, and offered higher manipulation speeds. On the other hand, the trapping mechanism in MNT-D2 was primarily electromagnetic in nature with minimal thermal effects and was therefore applicable to colloidal particles of any S_T, although with reduced propulsion speeds (≤1 μm/s).

The dependence of trapping efficiency on optical power and rotation speed provided a unique application possibility that does not exist with plasmonic tweezers or microrobots individually but is made possible because of the confluence of the two independent manipulation techniques. Figure 3A shows a size-based sorting scheme. Two beads of unequal sizes are trapped on an MNT. The smaller bead could be released by reducing the illumination intensity, and the MNT could thereby selectively transport the larger bead (Fig. 3B and movie S4). Alternately, by choosing an appropriate rotation frequency, the larger bead can be released because it experiences higher drag and is therefore ejected at a lower speed (movie S5). This is in accordance with the size dependence of Ω_{max} shown in Fig. 2E. The smaller bead can then be carried to a different location, as shown in Fig. 3C. The limitations of current technologies for microfluidic sorting would allow either the largest or the smallest species to be transported, whereas the MNTs could be used to trap and transport the cargo of varying sizes by combining manipulation techniques.

We used MNTs to maneuver a wide variety of colloidal materials beyond standard silica and PS beads. As shown in Fig. 4A, a biological material (submicrometer-size *Staphylococcus aureus* bacteria) was trapped and transported and then subsequently released by turning the illumination off (movie S6). The typical illumination intensities used in our experiments were almost two orders of magnitude lower than the optical intensity (~1800 kW/cm^2) that can damage living bacteria (*35*). In certain cases, by choosing materials with appropriate surface properties, it was possible to attach the colloidal cargo permanently, such as with fluorescent nanodiamonds, which are promising

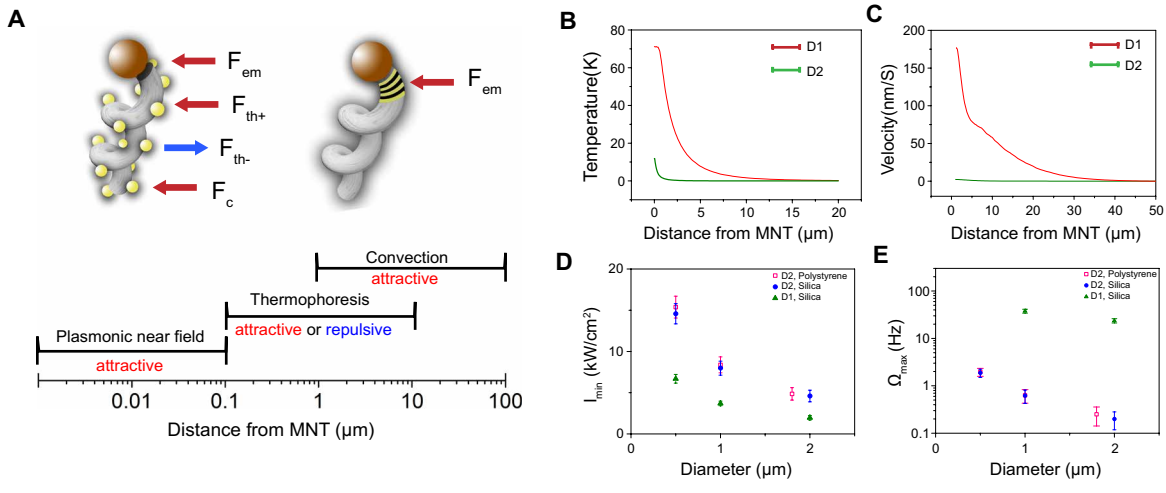

Fig. 2. Trapping mechanism and differences between the designs. (**A**) Schematic of the different forces acting on MNT-D1 and MNT-D2 showing length scales at which the forces dominate. The electromagnetic near field generates trapping forces (**F_{em}**) very close (<100 nm) to both MNT designs, whereas the thermophoretic (**F_{th}**) and convective (**F_c**) forces are only present with design D1. The magnitude of **F_{th}** depends on the spatial gradient of temperature and is appreciable within a few micrometers from the MNT-D1, whereas the convective flow can exist up to 100 μm away. (**B**) Calculated temperature and (**C**) convective flow velocity as function of distance from the MNT. (**D**) Minimum illumination intensity to trap as a function of bead size and material (PS and silica) for the two designs. (**E**) Maximum angular frequency of the MNT-bead system as a function of bead size for a fixed intensity (22 kW/cm^2). Error bars represent SD.

candidates for cutting-edge biomedical (*36*) and electronic (*37*) applications. As shown in Fig. 4B, the carboxyl-functionalized nanodiamonds (average diameter, 120 nm; Sigma-Aldrich), which have affinity to noble metals (*38*, *39*), were optically trapped by the MNT and thereafter were permanently attached to the MNT surface. Once attached, the MNT-nanodiamond system was maneuvered in three dimensions (movie S7), and the nanodiamonds remained attached to the MNT even when the illumination was reduced to zero. We have also performed experiments with nonfunctionalized nanodiamonds (shown in fig. S8) showing cargo release by lowering the optical intensity, similar to the colloidal beads and bacteria described before. Our technique permits accurate positioning of the MNT-cargo complex at specific locations on a substrate, which can be useful in realizing many applications envisioned with nanodiamonds (*40*).

We present (Fig. 5) two schemes to demonstrate how MNTs can be used for nanoscale assembly and how they offer greater speed and versatility compared with existing techniques. In the first scheme (Fig. 5A), we compare the passive diffusion of a colloidal cargo into a trap with the case where the cargo is actively loaded into the trap by the MNT. Assuming the initial distance of the cargo from the trap to be L, the improvement in loading time is vL/D, where v is the speed of the MNT and D is the diffusion constant of the cargo. A demonstration with an optical trap and two colloidal particles located about 50 μm away from the trap is shown in Fig. 5B. The MNT selectively carried one of the particles and subsequently loaded the trap, whereas the other particle remained at approximately the same position. The total time taken was 40 s, which demonstrates an improvement by a factor of 130 in comparison to passive diffusion. In Fig. 5C, the MNT is shown to load

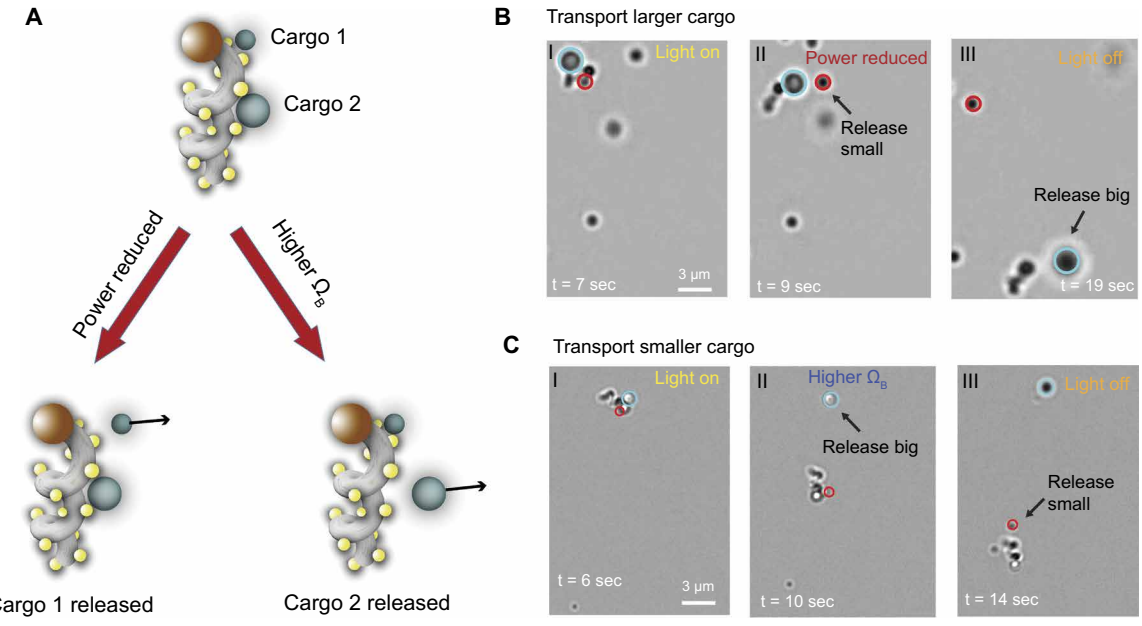

Fig. 3. Size-selective transport by varying optical intensity and speed. (**A**) Two ways to transport beads selected by size. By reducing the power, the smaller bead can be released, whereas increasing the frequency would release the larger bead. (**B**) Selectively transporting a 2-μm silica bead (1 μm released) using an optical intensity of 12 kW/cm^2. (**C**) Selectively transporting a 500-nm PS bead and releasing a 1-μm bead by maneuvering the MNT at 1 Hz.

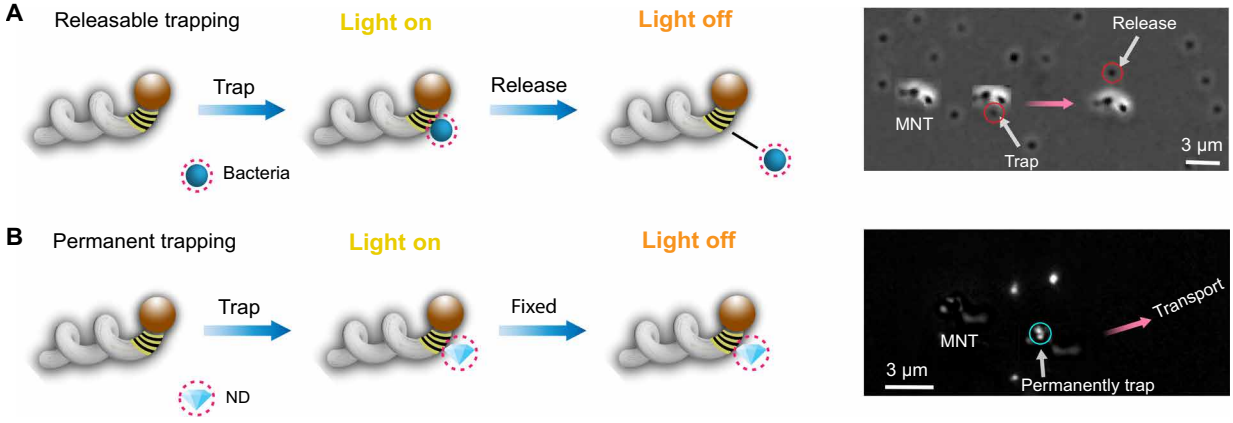

Fig. 4. Releasable and permanent trapping. (**A**) Biological materials—here, bacteria (*S. aureus*)—could be trapped and transported under an illumination of 30 kW/cm^2 and subsequently released upon removal of the illumination, as with the silica and PS beads. (**B**) Fluorescent nanodiamonds were permanently attached to the MNT under an optical illumination of 50 kW/cm^2 and subsequently manipulated.

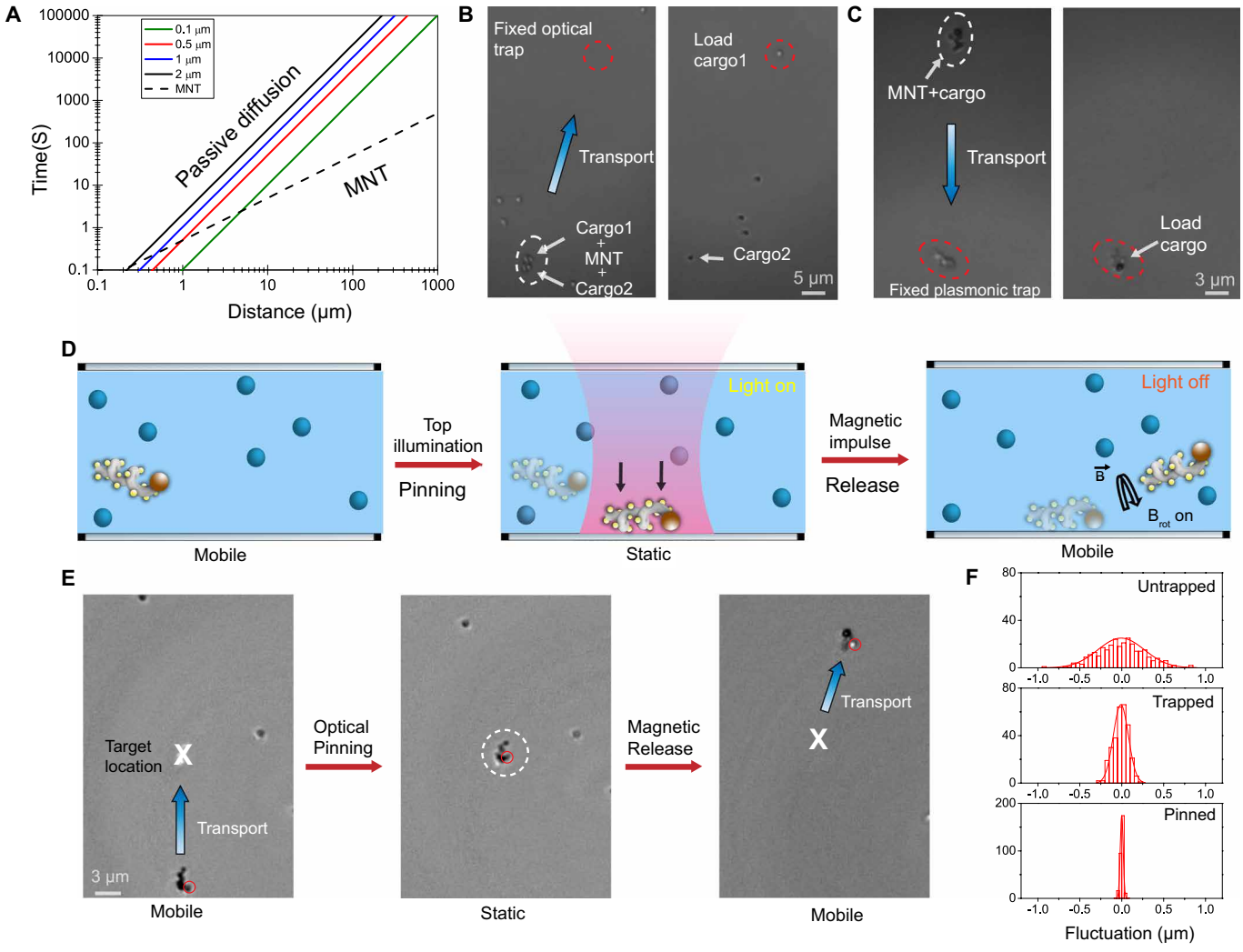

Fig. 5. Schemes of nanoscale assembly. Scheme 1: MNTs for accurate and fast loading of cargo into existing traps. (**A**) Time required by MNT in bringing cargo to a trap (dashed line) compared with passive diffusion (solid lines for different cargo sizes) from varying distances. We assume that the MNT-cargo complex is moving at 2 μm/s. (**B** and **C**) MNT loading a conventional optical trap (B) and a plasmonic trap (C). **Scheme 2:** (**D**) Schematic of optomechanically controlled positioning of the MNT. (**E**) Static and dynamic nanotweezing, with pinning-unpinning of the MNT on the chamber surface controlled by radiation pressure and magnetic fields. (**F**) Histogram of fluctuations for an untrapped bead (without laser illumination), along with beads trapped on MNT suspended in a fluid and on MNT pinned to a substrate.

a plasmonic trap; here, an optically printed MNT. Standard plasmonic tweezers are speed-limited by the slow, random diffusion of the cargo. Previous efforts to improve speeds of standard plasmonic tweezers either required invasive optical fibers with limited range of motion (<15 μm) (*41*) or the application of modulated electric fields within a customized microfluidic chamber (*12*). The solution provided here greatly speeds up the trapping process without compromising the generality of plasmonic tweezers as applied to a wide variety of materials and fluids (*42*).

An alternate scheme to accurately position nano-objects, demonstrating the versatility of MNTs, is shown in Fig. 5D, where an MNT can be made static by optically pushing and therefore "printing" (*43*) it onto the substrate (movie S8). This was done by adding an illumination of 250 kW/cm^2 from the top of the chamber, where the strong radiation pressure pushes and binds the MNT onto the substrate. Crucially, the MNTs could later be released from the substrate by reducing the optical power and momentarily applying a high magnetic field (~200 G) in slow (~1 Hz) rotating configuration. By pinning and unpinning the MNT using optical and magnetic fields, we could attach a plasmonic tweezer to any spot on the chamber without requiring prior nanopatterning. Additionally, the pinning-unpinning manipulations could be carried out even with the cargo trapped on the MNT, as shown in Fig. 5E.

Last, we demonstrated the levels of localization achievable with the MNTs (Fig. 5F). The histogram of position fluctuations of a 500-nm bead trapped on a pinned and an unpinned MNT shows much higher localization in comparison to an untrapped bead. The fluctuations of the bead on the unpinned MNT arise because of thermal fluctuations of the suspended helix, which in turn depend on the size of the MNT. The bead on the pinned MNT was strongly localized, as would be expected in a standard plasmonic tweezer.

CONCLUSIONS

The class of optical nanomanipulators described here can be operated remotely and noninvasively to trap, transport, release, and position the cargo in fluidic environments. This was achieved by combining two

technologies of current interest, plasmonically enhanced trapping integrated with artificial microrobots that can be externally controlled with small magnetic fields. This technique is general enough to be applicable to both thermophilic (silica) and thermophobic (PS) materials, despite their opposite response to thermal gradients. The MNTs described can be mass-produced and thereafter integrated seamlessly in standard lab-on-chip systems, such as to carry out colloidal manipulation tasks, including biological materials and nanodiamonds. By using different magnetic field configurations, it may be possible to maneuver multiple MNTs autonomously (*44*) or along independent directions (*45*), which may allow parallelizing the transport and sorting capabilities demonstrated here. We envision the MNTs to be particularly useful in applications pertaining to hybrid nanoscale assembly, because it offers freedom and versatility that surpasses the capabilities of existing nanomanipulation techniques.

MATERIALS AND METHODS

Fabrication and characterization of the MNTs

We used a Langmuir-Blodgett trough (Apex Instruments) to deposit a monolayer of colloidal beads (made of PS) on a substrate, which is depicted as a sphere in Fig. 1A. We incorporated different materials in a layer-by-layer evaporation scheme on the individual beads using glancing angle deposition, where the substrate was kept at an extreme angle with respect to the source of evaporated material.

First, we describe the method followed to fabricate MNT-D1. Initially, the substrate was kept stationary, and we deposited a 5-nm layer of Ag, followed by 60 nm of Fe and another 5 nm of Ag. This was followed by growing a film of SiO_2 by rotating the substrate slowly at one revolution per hour per micrometer of deposited silica, resulting in the formation of a helical nanostructure. The role of Ag was twofold, serving both as an adhesion promoter between the ferromagnetic Fe and the SiO_2 helix and as a plasmonic nanoantenna to couple the incident light. To further enhance its plasmonic properties, we deposited a thin film (5 nm) of Ag on the MNT film, followed by annealing at 300°C for 1 min to dewet the film and form Ag nanoislands. This resulted in many plasmonic nanoparticles around the helix, resulting in a maximum absorption wavelength of around 450 nm (see the Supplementary Materials).

To fabricate MNT-D2, we performed layer-by-layer deposition of Ag and Fe (10 and 20 nm thick, respectively), with three layers of Ag and two layers of Fe in between (fig. S9B). This was followed by growing a film of SiO_2 where the substrate was rotated slowly at one revolution per hour per micrometer of deposited silica, resulting in the formation of a helical nanostructure. Our fabrication method is wafer-scale with a yield of about 10^8 MNT-D2 nanostructures cm^{-2}.

Experimental setup and methodology

The experimental setup is shown in fig. S1. A triaxial Helmholtz coil was built around an optical microscope to generate the rotating magnetic field. The substrate containing the MNTs was sonicated in deionized water, and subsequently, we prepared a fluidic suspension containing both MNTs and the colloidal particles. The experiments were carried out inside a microfluidic chamber of thickness between 5 and 20 μm made by sandwiching two glass slides, where the MNTs typically stabilized close to the bottom wall of the chamber. All the experiments were carried out in deionized water at 25°C. A defocused laser beam with a wavelength of 447 nm was used to illuminate an approximate area between 100 and 1000 μm^2. This resulted in a radiation pressure (~50 fN at 20 kW/cm^2 for MNT-D2) that pushed the MNT toward the chamber walls and was stabilized by electrostatic repulsion from the glass surface. Also relevant is the force due to magnetic drive. Assuming translational diffusivity to be 0.5 $\mu m^2/s$ (*46*), the effective drag required to be overcome by the external magnetic drive is about 16 fN for an MNT moving at 2 μm/s. The available magnetic force can be made larger by driving at higher speeds. We previously defined the experimental methodology in Results (see also Fig. 2).

The optical printing of MNTs on the substrate was achieved in a slightly different setup where we illuminated the chamber from the top. When the strong radiation pressure was larger than the electrostatic repulsion of the bottom glass substrate, the MNT was immobilized, which was achieved for optical illumination intensity larger than 200 kW/cm^2. A relatively large magnetic field (~200 G) that generated enough force (~ pN) to release the MNT adhered on the substrate was applied.

Control experiments

We performed experiments with silica helices (i.e., no plasmonic material) and colloidal beads under high laser intensities where we did not observe any trapping. In addition, we checked the role of nonresonant illumination at 1064 nm with MNT-D1, where heat generated and therefore thermofluidic effects are expected to be reduced or absent, and we did not observe any trapping up to a laser illumination intensity of 20 kW/cm^2.

Dynamics of the MNTs

At low frequencies, the MNTs showed precession dynamics (movie S5). This could be understood from the dynamics of elongated objects under external torque at low Reynolds numbers, which have been addressed extensively in a previous study from our group (*47*). The precessional motion arises because of balance between the applied magnetic torque and the viscous drag experienced by the rotating helix at a certain dynamical configuration. In addition, the MNTs show Brownian motion that has been investigated and successfully modeled in a previous paper (*46*).

SUPPLEMENTARY MATERIALS

robotics.sciencemag.org/cgi/content/full/3/14/eaaq0076/DC1

Fig. S1. Schematic of the experimental setup.
Fig. S2. Radial profile of the illumination intensity.
Fig. S3. Optical transmission data for MNT-D1 peaking around the laser wavelength of 447 nm.
Fig. S4. Interparticle spacing and size distribution for MNT-D1.
Fig. S5. Role of thermal effects.
Fig. S6. Histogram of position fluctuations for an untrapped bead.
Fig. S7. Minimum intensity required for trapping 1-μm beads versus time.
Fig. S8. Trap and release of nonfunctionalized nanodiamond.
Fig. S9. Geometry used in our numerical model.
Fig. S10. Electric field intensity enhancement.
Fig. S11. Geometry for simulation.
Fig. S12. Convective velocity pattern and increased temperature distribution around MNT-D2.
Fig. S13. Convective velocity pattern and increased temperature distribution around MNT-D1.
Fig. S14. Experimental estimation of trapping force.
Fig. S15. Theoretical estimation of trapping force.
Movie S1. Demonstration of trapping and transport of silica beads of diameter 1 and 2 μm over a distance of 22 μm using MNT-D1.
Movie S2. Demonstration of trapping and releasing of silica beads of diameter 150 nm using MNT-D1.
Movie S3. Demonstrating superior spatio-temporal control over particle manipulation by tracing out the letter "N" with MNT-D1.
Movie S4. Size selective transport of 2 μm Silica beads using MNT-D1.

Movie S5. Size selective transport of 500 nm PS beads using MNT-D2.
Movie S6. Demonstration of trapping and releasing of sub-micron size bacteria (*Staphylococcus aureus*) using MNT-D2.
Movie S7. Demonstration of trapping and 3D-transport of 120 nm fluorescent nanodiamonds using MNT-D2.
Movie S8. Demonstration of pinning-depinning mechanism with MNT-D1.
References (*48*–*56*)

REFERENCES AND NOTES

1. O. Benson, Assembly of hybrid photonic architectures from nanophotonic constituents. *Nature* **480**, 193–199 (2011).
2. A. Ashkin, J. M. Dziedzic, J. E. Bjorkholm, S. Chu, Observation of a single-beam gradient force optical trap for dielectric particles. *Opt. Lett.* **11**, 288–290 (1986).
3. J. Shi, D. Ahmed, X. Mao, S.-C. S. Lin, A. Lawit, T. J. Huang, Acoustic tweezers: Patterning cells and microparticles using standing surface acoustic waves (SSAW). *Lab Chip.* **9**, 2890–2895 (2009).
4. F. H. C. Crick, A. F. W. Hughes, The physical properties of cytoplasm: A study by means of the magnetic particle method. Part I. Experimental. *Exp. Cell Res.* **1**, 37–80 (1950).
5. D. L. Fan, F. Q. Zhu, R. C. Cammarata, C. L. Chien, Electric tweezers. *Nano Today* **6**, 339–354 (2011).
6. T. Petit, L. Zhang, K. E. Peyer, B. E. Kratochvil, B. J. Nelson, Selective trapping and manipulation of microscale objects using mobile microvortices. *Nano Lett.* **12**, 156–160 (2012).
7. M. Righini, A. S. Zelenina, C. Girard, R. Quidant, Parallel and selective trapping in a patterned plasmonic landscape. *Nat. Phys.* **3**, 477–480 (2007).
8. A. N. Grigorenko, N. W. Roberts, M. R. Dickinson, Y. Zhang, Nanometric optical tweezers based on nanostructured substrates. *Nat. Photonics* **2**, 365–370 (2008).
9. Y. Pang, R. Gordon, Optical trapping of a single protein. *Nano Lett.* **12**, 402–406 (2012).
10. O. M. Maragò, P. H. Jones, P. G. Gucciardi, G. Volpe, A. C. Ferrari, Optical trapping and manipulation of nanostructures. *Nat. Nanotechnol.* **8**, 807–819 (2013).
11. T. Shoji, Y. Tsuboi, Plasmonic optical tweezers toward molecular manipulation: Tailoring plasmonic nanostructure, light source, and resonant trapping. *J. Phys. Chem. Lett.* **5**, 2957–2967 (2014).
12. J. C. Ndukaife, A. V. Kildishev, A. G. A. Nnanna, V. M. Shalaev, S. T. Wereley, A. Boltasseva, Long-range and rapid transport of individual nano-objects by a hybrid electrothermoplasmonic nanotweezer. *Nat. Nanotechnol.* **11**, 53–59 (2016).
13. J. Wang, *Nanomachines: Fundamentals and Applications* (John Wiley & Sons, 2013).
14. W. F. Paxton, K. C. Kistler, C. C. Olmeda, A. Sen, S. K. St. Angelo, Y. Cao, T. E. Mallouk, P. E. Lammert, V. H. Crespi, Catalytic nanomotors: Autonomous movement of striped nanorods. *J. Am. Chem. Soc.* **126**, 13424–13431 (2004).
15. S. Fournier-Bidoz, A. C. Arsenault, I. Manners, G. A. Ozin, Synthetic self-propelled nanorotors. *Chem. Commun.* **4**, 441–443 (2005).
16. A. Ghosh, P. Fischer, Controlled propulsion of artificial magnetic nanostructured propellers. *Nano Lett.* **9**, 2243–2245 (2009).
17. P. Fischer, A. Ghosh, Magnetically actuated propulsion at low Reynolds numbers: Towards nanoscale control. *Nanoscale* **3**, 557–563 (2011).
18. L. Zhang, J. J. Abbott, L. Dong, B. E. Kratochvil, D. Bell, B. J. Nelson, Artificial bacterial flagella: Fabrication and magnetic control. *Appl. Phys. Lett.* **94**, 064107 (2009).
19. J. Wang, Cargo-towing synthetic nanomachines: Towards active transport in microchip devices. *Lab Chip* **12**, 1944–1950 (2012).
20. J. Li, B. Esteban-Fernández de Ávila, W. Gao, L. Zhang, J. Wang, Micro/nanorobots for biomedicine: Delivery, surgery, sensing, and detoxification. *Sci. Robot.* **2**, eaam6431 (2017).
21. S. Sundararajan, P. E. Lammert, A. W. Zudans, V. H. Crespi, A. Sen, Catalytic motors for transport of colloidal cargo. *Nano Lett.* **8**, 1271–1276 (2008).
22. J. Burdick, R. Laocharoensuk, P. M. Wheat, J. D. Posner, J. Wang, Synthetic nanomotors in microchannel networks: Directional microchip motion and controlled manipulation of cargo. *J. Am. Chem. Soc.* **130**, 8164–8165 (2008).
23. T.-Y. Huang, M. S. Sakar, A. Mao, A. J. Petruska, F. Qiu, X.-B. Chen, S. Kennedy, D. Mooney, B. J. Nelson, 3D printed microtransporters: Compound micromachines for spatiotemporally controlled delivery of therapeutic agents. *Adv. Mater.* **27**, 6644–6650 (2015).
24. T.-Y. Huang, F. Qiu, H.-W. Tung, X.-B. Chen, B. J. Nelson, M. S. Sakar, Generating mobile fluidic traps for selective three-dimensional transport of microobjects. *Appl. Phys. Lett.* **105**, 114102 (2014).
25. Q. Zhou, T. Petit, H. Choi, B. J. Nelson, L. Zhang, Dumbbell fluidic tweezers for dynamical trapping and selective transport of microobjects. *Adv. Funct. Mater.* **27**, 1604571 (2017).
26. E. M. Purcell, Life at low Reynolds number. *Am. J. Phys.* **45**, 3–11 (1977).
27. O. Felfoul, M. Mohammadi, S. Taherkhani, D. de Lanauze, Y. Z. Xu, D. Loghin, S. Essa, S. Jancik, D. Houle, M. Lafleur, L. Gaboury, M. Tabrizian, N. Kaou, M. Atkin, T. Vuong, G. Batist, N. Beauchemin, D. Radzioch, S. Martel, Magneto-aerotactic bacteria deliver drug-containing nanoliposomes to tumour hypoxic regions. *Nat. Nanotechnol.* **11**, 941–947 (2016).
28. B. J. Roxworthy, A. M. Bhuiya, S. P. Vanka, K. C. Toussaint Jr., Understanding and controlling plasmon-induced convection. *Nat. Commun.* **5**, 3173 (2014).
29. R. Piazza, 'Thermal forces': Colloids in temperature gradients. *J. Phys. Condens. Matter* **16**, S4195–S4211 (2004).
30. F. M. Weinert, D. Braun, Observation of slip flow in thermophoresis. *Phys. Rev. Lett.* **101**, 168301 (2008).
31. A. Cuche, A. Canaguier-Durand, E. Devaux, J. A. Hutchison, C. Genet, T. W. Ebbesen, Sorting nanoparticles with intertwined plasmonic and thermo-hydrodynamical forces. *Nano Lett.* **13**, 4230–4235 (2013).
32. S. Y. Kim, J. D. Taylor, H. D. Ladouceur, S. J. Hart, A. Terray, Radiation pressure efficiency measurements of nanoparticle coated microspheres. *Appl. Phys. Lett.* **103**, 234101 (2013).
33. S. Divitt, L. Rondin, L. Novotny, Cancellation of non-conservative scattering forces in optical traps by counter-propagating beams. *Opt. Lett.* **40**, 1900–1903 (2015).
34. A. van der Horst, P. D. J. van Oostrum, A. Moroz, A. van Blaaderen, M. Dogterom, High trapping forces for high-refractive index particles trapped in dynamic arrays of counterpropagating optical tweezers. *Appl. Opt.* **47**, 3196–3202 (2008).
35. M. B. Rasmussen, L. B. Oddershede, H. Siegumfeldt, Optical tweezers cause physiological damage to *Escherichia coli* and *Listeria* bacteria. *Appl. Environ. Microbiol.* **74**, 2441–2446 (2008).
36. X. Chen, W. Zhang, Diamond nanostructures for drug delivery, bioimaging, and biosensing. *Chem. Soc. Rev.* **46**, 734–760 (2017).
37. R. Schirhagl, K. Chang, M. Loretz, C. L. Degen, Nitrogen-vacancy centers in diamond: Nanoscale sensors for physics and biology. *Annu. Rev. Phys. Chem.* **65**, 83–105 (2014).
38. M. Geiselmann, R. Marty, J. Renger, F. J. García de Abajo, R. Quidant, Deterministic optical-near-field-assisted positioning of nitrogen-vacancy centers. *Nano Lett.* **14**, 1520–1525 (2014).
39. H. Sellers, A. Ulman, Y. Shnidman, J. E. Eilers, Structure and binding of alkanethiolates on gold and silver surfaces: Implications for self-assembled monolayers. *J. Am. Chem. Soc.* **115**, 9389–9401 (1993).
40. J. T. Kim, U. Choudhury, H.-H. Jeong, P. Fischer, Nanodiamonds that swim. *Adv. Mater.* **29**, 1701024 (2017).
41. J. Berthelot, S. S. Aćimović, M. L. Juan, M. P. Kreuzer, J. Renger, R. Quidant, Three-dimensional manipulation with scanning near-field optical nanotweezers. *Nat. Nanotechnol.* **9**, 295–299 (2014).
42. B. J. Roxworthy, M. T. Johnston, F. T. Lee-Montiel, R. H. Ewoldt, P. I. Imoukhuede, K. C. Toussaint Jr., Plasmonic optical trapping in biologically relevant media. *PLOS ONE* **9**, e93929 (2014).
43. A. S. Urban, A. A. Lutich, F. D. Stefani, J. Feldmann, Laser printing single gold nanoparticles. *Nano Lett.* **10**, 4794–4798 (2010).
44. P. Mandal, A. Ghosh, Observation of enhanced diffusivity in magnetically powered reciprocal swimmers. *Phys. Rev. Lett.* **111**, 248101 (2013).
45. P. Mandal, V. Chopra, A. Ghosh, Independent positioning of magnetic nanomotors. *ACS Nano* **9**, 4717–4725 (2015).
46. A. Ghosh, D. Paria, G. Rangarajan, A. Ghosh, Velocity fluctuations in helical propulsion: How small can a propeller be. *J. Phys. Chem. Lett.* **5**, 62–68 (2014).
47. A. Ghosh, D. Paria, H. J. Singh, P. L. Venugopalan, A. Ghosh, Dynamical configurations and bistability of helical nanostructures under external torque. *Phys. Rev. E Stat. Nonlin. Soft Matter Phys.* **86**, 031401 (2012).
48. K. Wang, E. Schonbrun, P. Steinvurzel, K. B. Crozier, Trapping and rotating nanoparticles using a plasmonic nano-tweezer with an integrated heat sink. *Nat. Commun.* **2**, 469 (2011).
49. S. Duhr, D. Braun, Why molecules move along a temperature gradient. *Proc. Natl. Acad. Sci. U.S.A.* **103**, 19678–19682 (2006).
50. R. Piazza, A. Parola, Thermophoresis in colloidal suspensions. *J. Phys. Condens. Matter* **20**, 153102 (2008).
51. T. Shoji, M. Shibata, N. Kitamura, F. Nagasawa, M. Takase, K. Murakoshi, A. Nobuhiro, Y. Mizumoto, H. Ishihara, Y. Tsuboi, Reversible photoinduced formation and manipulation of a two-dimensional closely packed assembly of polystyrene nanospheres on a metallic nanostructure. *J. Phys. Chem. C* **117**, 2500–2506 (2013).
52. D. Y. Smith, E. Shiles, M. Inokuti, in *Handbook of optical constants of solids*, E. D. Palik, Ed. (Academic Press, 1985), vol. 1, pp. 369–406.
53. W. S. M. Werner, K. Glantschnig, C. Ambrosch-Draxl, Optical constants and inelastic electron-scattering data for 17 elemental metals. *J. Phys. Chem. Ref. Data* **38**, 1013–1092 (2009).
54. E. Guyon, *Physical Hydrodynamics* (Oxford Univ. Press, 2001).
55. G. Baffou, P. Berto, E. Bermúdez Ureña, R. Quidant, S. Monneret, J. Polleux, H. Rigneault, Photoinduced heating of nanoparticle arrays. *ACS Nano* **7**, 6478–6488 (2013).

56. G. Baffou, R. Quidant, F. J. García de Abajo, Nanoscale control of optical heating in complex plasmonic systems. *ACS Nano* **4**, 709–716 (2010).

Acknowledgments: We gratefully acknowledge the help from D. Paria, D. Saini, H. Kakoty, J. H. Singh, P. Mandal, S. Pandit, P. Prakash, S. S. Gorthy, V. Balaswamy, and V. R. Supradeepa and the usage of the facilities available in the Micro and Nano Characterization Facility at the Centre for Nano Science and Engineering, Indian Institute of Science. **Funding:** This work is supported by Nano Mission and the Science and Engineering Research Board, Government of India. This work is partially supported by the Ministry of Communication and Information Technology under a grant for the Centre of Excellence in Nanoelectronics, Phase II.
Author contributions: A.G. conceived and supervised the work. S.G. built the numerical model and the optical setup and performed the experiments and numerical simulations. Both authors brainstormed and discussed extensively during this research work and prepared the manuscript together. **Competing interests:** The authors declare that they have no competing interests. **Data and materials availability:** All data to support the conclusions of this manuscript are included in the main text or the Supplementary Materials. Requests for all materials should be addressed to A.G.

Submitted 22 September 2017
Accepted 4 December 2017
Published 10 January 2018
10.1126/scirobotics.aaq0076

Citation: S. Ghosh, A. Ghosh, Mobile nanotweezers for active colloidal manipulation. *Sci. Robot.* **3**, eaaq0076 (2018).

Science Robotics

Mobile nanotweezers for active colloidal manipulation

Souvik Ghosh and Ambarish Ghosh

Sci. Robot. **3** (14), eaaq0076. DOI: 10.1126/scirobotics.aaq0076

Science Robotics (ISSN 2470-9476) is published by the American Association for the Advancement of Science. 1200 New York Avenue NW, Washington, DC 20005. The title *Science Robotics* is a registered trademark of AAAS.